Journal of
Marine Science and Engineering

MDPI

Article

Proportioning Test on the Similar Materials of the Rock Mass Physical Model Test Considering Seepage and Dynamic Characteristics

Wanpeng Shi [1], Jianwei Zhang [1], Chunlei Xin [2], Danqing Song [3,*], Nan Hu [4] and Bowei Li [4]

[1] School of Civil Engineering and Architecture, Henan University, Kaifeng 475000, China; zjw@henu.edu.cn (J.Z.)
[2] State Key Laboratory of Geohazard Prevention and Geoenvironment Protection, College of Environment and Civil Engineering, Chengdu University of Technology, Chengdu 610059, China; xinchunlei@cdut.edu.cn
[3] State Key Laboratory of Subtropical Building Science, School of Civil Engineering and Transportation, South China University of Technology, Guangzhou 510640, China
[4] State Key Laboratory of Hydroscience and Engineering, Tsinghua University, Beijing 100084, China; hunan0427@mail.tsinghua.edu.cn (N.H.); li-bw20@mails.tsinghua.edu.cn (B.L.)
* Correspondence: dqsong@scut.edu.cn

Abstract: With the development of infrastructure construction, an increasing number of projects are faced with the problem of hydraulic and dynamic coupling. However, traditional physical model materials mainly consider the single factor influence and lack comprehensive research on the hydraulic and dynamic parameters of similar materials. Based on the dimensionless criterion and Buckingham π theorem, the dimension and similarity relation of physical model tests of rock masses under seepage and dynamic coupling are derived. A new type of similar material considering hydraulic and dynamic properties was developed by using quartz sand, barite powder, cement, water glass, rosin, and glycerol as raw materials through a large number of orthogonal tests. Meanwhile, the sensitivity analysis of the physical and mechanical properties of similar materials was carried out and the influence of each component factor on the physical properties was revealed. A material preparation scheme was developed to meet the physical and hydraulic characteristics of different rock and soil physical models. An empirical matching formula considering each parameter is proposed. This work can provide an important reference for physical model tests of similar rock masses.

Keywords: model test; percolation–dynamic coupling; similarity relation; orthogonal test; similar material; sensitivity analysis; empirical equations

Citation: Shi, W.; Zhang, J.; Xin, C.; Song, D.; Hu, N.; Li, B. Proportioning Test on the Similar Materials of the Rock Mass Physical Model Test Considering Seepage and Dynamic Characteristics. *J. Mar. Sci. Eng.* **2023**, *11*, 1815. https://doi.org/10.3390/jmse11091815

Academic Editor: Dimitris Sakellariou

Received: 11 August 2023
Revised: 8 September 2023
Accepted: 15 September 2023
Published: 18 September 2023

1. Introduction

With the rapid development of national economic construction, basic projects such as water conservancy and hydropower, transportation, and energy mines have gradually developed [1]. In the process of development, each project also gradually encountered some complex engineering geological problems (hydraulic–dynamic coupling problems) [2]. For example, traffic construction has gradually shifted from plain areas to mountainous, hilly, and coastal areas [3]. Tunnels in mountainous areas often face complex geological structures, frequent earthquakes, and concentrated heavy rainfall phenomena [4,5] which are prone to problems such as water inrush and landslides. With the development and utilization of marine resources, problems such as hydraulic change [6], wave shock [7], and plate vibration [8] are often encountered in the process of ocean construction. Water conservancy and hydropower projects have often been affected by earthquakes and reservoir drainage since their construction [9]. Coal mine projects are prone to water inrush, mud outbursts, and collapse accidents in water-rich areas [10]. With the development of energy cleanliness, underground reservoirs are gradually built in coal mines in arid areas which are highly

sensitive to mine earthquakes and water action [11]. Figure 1 shows some of the disasters caused by hydraulic–dynamic coupling in various fields.

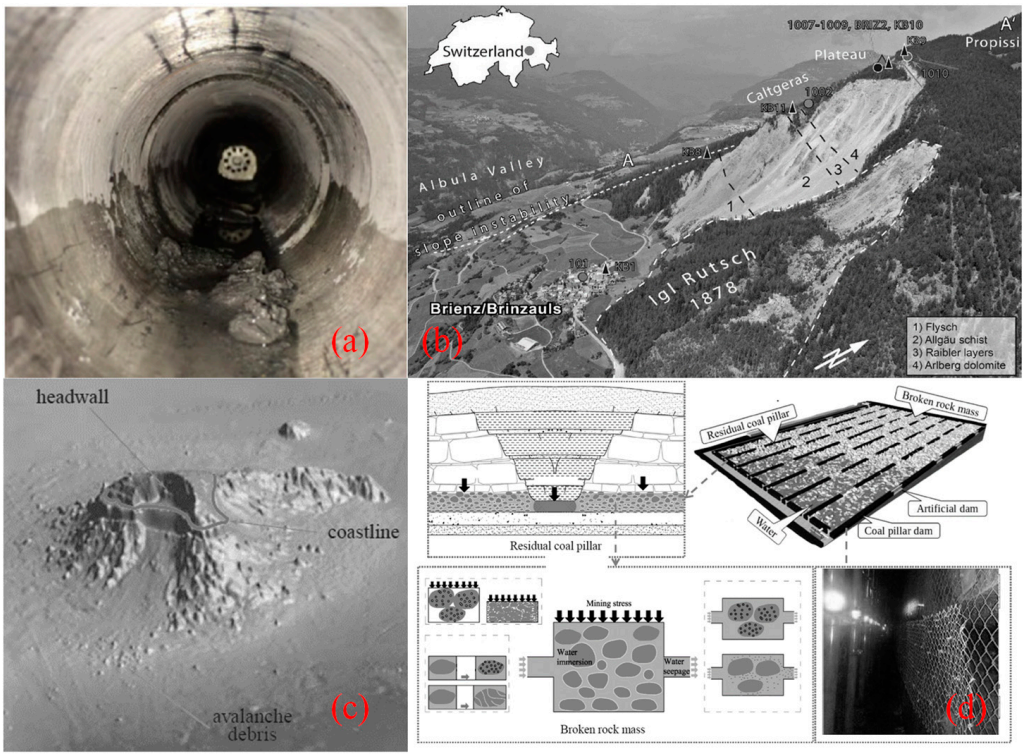

Figure 1. Tunnel and slope disasters: (**a**) water gushing from the tunnel [1]; (**b**) slope disaster under earthquake and rain [5]; (**c**) submarine landslide [7]; and (**d**) coal mine underground reservoir damage [11].

In summary, an increasing number of engineering projects are facing the problem of multi-field coupling. Some scholars have used fiber concrete to improve the properties of engineering materials [12,13]. Some scholars also use low-strength materials as backfill or high-strength materials in coal mines [14–16]. However, the study of the above materials is considered from the perspective of protection and reinforcement and has no reference significance for the stability analysis and instability mechanism under hydraulic and dynamic action. At present, theoretical analysis [7], numerical simulation [17], and physical model tests [18] have become the main research methods to study the above problems, aiming at engineering problems such as the disaster evolution process, stability analysis, and prevention and control of complex rock mass under hydraulic–dynamic coupling. Nevertheless, the theoretical analysis requires many simplifications and assumptions of the prototype, which is not suitable for the study of complex geological problems. The study of the damage evolution mechanism by numerical simulation is limited and verification by model tests and field tests is lacking [9]. Additionally, the physical model test has become an important method to study the disaster mechanism of engineering rock masses under complex conditions because it can truly restore the failure evolution process and instability mode of complex rock masses [18]. In particular, accurately obtaining the similarity between similar materials and real rock mass materials becomes the key to accurately reflecting the failure process of rock mass model tests [19]. This work intends to use physical model tests to study engineering problems under hydraulic–dynamic action so research on new similar materials is an important basic work at present.

Meanwhile, many scholars have carried out relevant research on similar materials of rock mass physical modes. Some scholars have used MLPS or gypsum to study the anchorage characteristics and crack propagation of rock-like materials [20,21] but the above

studies are based on certain materials in specific engineering studies rather than a class of similar materials with a wide range of changes.

In consideration of the parameter range and characteristics of similar materials, Li et al. [22,23] developed a series of new fluid–structure coupling materials such as SCVO and PSTO based on the fluid–structure coupling similarity theory of continuous media. Shen et al. [6] developed a similar material suitable for sand formation conditions in deep-sea environments by using standard sand, petroleum jelly, and other materials. Zhang et al. [19] derived similar criteria for fluid–solid coupling under high osmotic pressure and high ground stress and developed a new fluid–solid coupling material with white cement, silicone oil, and other materials. However, the above similar materials are prepared with paraffin, silicone oil, petroleum jelly, and other oily liquids, so it is difficult to avoid the use of alcohol lamps for heating and melting treatment which can easily cause danger. Furthermore, Xu et al. [24] successfully developed similar materials suitable for simulating the development and evolution of tunnel lining cracks by using gypsum, quartz sand, diatomite, and fly ash. Wang et al. [25], based on the Xianglushan tunnel, developed similar materials that could simulate the failure modes of concrete and rock masses. But Xu and Wang's paper only discussed the failure mode of similar materials and the instability state of tunnel lining and did not consider the hydraulic and dynamic characteristics of similar materials. Additionally, some scholars have developed a series of similar materials suitable for fluid–structure coupling models using conventional materials such as quartz sand, cement, gypsum, and barite powder and successfully applied them to the simulation of cretaceous sandstone aquifer [26], red layer soft rock simulation [27], karst landform, and other physical model tests [28]. However, the above model tests only consider the permeability coefficient and the conventional physical and mechanical parameters. In terms of the dynamics of similar materials, Li et al. [29] and Tian et al. [30] conducted dynamic and static tests on rock samples composed of quartz sand, cement, and other materials but failed to deeply explore the hydrodynamic characteristics and the evolution law of dynamic parameters. At the same time, Cao et al. [18] and Yang et al. [31] designed and completed the shaking table model of slopes with weak interlayers under the action of rainfall. However, in the whole test process, only the saturation of the interlayer material was considered and the softening characteristics of the interlayer material in water and the change law of the dynamic parameters were ignored. Thus, there would be certain difficulties in the theoretical analysis in the later stage [32].

In summary, previous studies on similar materials have mainly focused on the physical and mechanical properties of materials under the influence of single factors such as seepage, dynamics, and failure phenomena. However, with the widespread occurrence of multi-field coupling phenomena such as hydraulic and dynamic fields, only studying the material properties of a single factor cannot meet the physical model test. Thus, it can be noted that the development of a new type of similar material that considers both hydraulic and dynamic properties is an urgent problem for the physical model test under multi-field coupling. Considering that traditional research on similar materials does not include both hydraulic and dynamic parameters, this work aims to obtain new similar materials. First, based on the dimensional analysis method and Buckingham π theorem, the similarity relationship of physical model tests under percolation–dynamic coupling is derived. Then, through an orthogonal test, with quartz sand and barite powder as aggregates, cement and sodium silicate as cementing materials, and rosin and glycerine as modulators, similar materials considering of both hydraulic and dynamic properties were developed. The sensitivity analysis and statistical analysis of the physical parameters and failure modes of specimens with different proportions were carried out. Finally, the fitting formulas of different parameters are obtained based on multiple regression analysis, which can provide a reliable basis for physical simulation tests of slopes or tunnels under the action of hydraulic and dynamic coupling.

2. Similarity Theory and Similarity Relation

According to the requirements of similarity theory, the coupling model test of statics, percolation, and dynamic field should satisfy the similarity of geometrical dimensions, mechanical properties, force conditions, hydraulic properties, and dynamic parameters. According to dimensional analysis, for any physical system, if it contains n physical quantities and k fundamental dimensions, the remaining (n-k) physical quantities can be expressed in fundamental dimensions [25,33].

The main physical quantities involved in the static percolation–dynamic field coupling model include the density ρ, geometric dimension L, elastic modulus E, Poisson's ratio μ, cohesion force c, internal friction angle φ, stress σ, strain ε, time t, frequency ω, displacement x, velocity v, acceleration a, gravitational acceleration g, damping ratio λ, dynamic elastic modulus Ed, dynamic Poisson's ratio μd, external force F, permeability coefficient k, and softening coefficient η for a total of 20 parameters. Meanwhile, the Poisson's ratio, internal friction angle, strain, damping ratio, dynamic Poisson's ratio, and softening coefficient are dimensionless parameters, that is Cμ, Cφ, Cε, Cλ, Cμd, and Cη are all 1. The experiment adopts an absolute dimension system with density ρ, geometric dimension L, and acceleration a as the basic dimensions. Then, the π function is

$$(\pi_1, \pi_2, \pi_3, \pi_4, \pi_5, \pi_6, \pi_7, \pi_8, \pi_9, \pi_{10}, \pi_{11}) = 0 \tag{1}$$

According to the method of dimensional analysis and Buckingham's π theorem, the general form of all physical parameters constituting the dimensionless π number is

$$\pi = E^a c^b \sigma^c t^d \omega^e x^f v^g g^h E_d{}^i F^j k^k \tag{2}$$

Substituting the dimensions of E, c, σ, t, ω, x, v, g, Ed, F, and k into Equation (2) yields

$$\begin{aligned} \pi = \left[M^0L^0T^0\right] &= \left[ML^{-1}T^{-2}\right]^a \left[ML^{-1}T^{-2}\right]^b \left[ML^{-1}T^{-2}\right]^c \left[M^0L^0T\right]^d \left[M^0L^0T^{-1}\right]^e \left[M^0L^1T^0\right]^f \\ &\quad \left[M^0L^1T^{-1}\right]^g \left[M^0L^1T^{-2}\right]^h \left[ML^{-1}T^{-2}\right]^i \left[ML^1T^{-2}\right]^j \left[M^0L^1T^{-1}\right]^k \\ &= \left[M^{a+b+c+i+j}\right] \left[L^{-a-b-c+f+g+h+i+j+k}\right] \left[T^{-2a-2b-2c+d-e-g-2h-2i-2j-k}\right] \end{aligned} \tag{3}$$

From the principle of dimensional consistency, similar invariants can be obtained by solving Equation (3):

$$\begin{gathered} \pi_1 = \frac{E}{\rho La} \quad \pi_2 = \frac{c}{\rho La} \quad \pi_3 = \frac{\sigma}{\rho La} \quad \pi_4 = \frac{t}{L^{0.5}a^{-0.5}} \quad \pi_5 = \frac{\omega}{L^{-0.5}a^{0.5}} \quad \pi_6 = \frac{x}{L} \\ \pi_7 = \frac{v}{L^{0.5}a^{0.5}} \quad \pi_8 = \frac{g}{a} \quad \pi_9 = \frac{E_d}{\rho La} \quad \pi_{10} = \frac{F}{\rho L^3 a} \quad \pi_{11} = \frac{k}{L^{0.5}a^{0.5}} \end{gathered} \tag{4}$$

In the derivation process, ρ, L, and a are determined as the basic dimensions and the similarity relationship of the remaining physical quantities is shown in Table 1.

In addition, because the percolation–dynamic coupling model is located in the gravitational field, $C_g = C_a = 1$; thus, the similar invariants of permeability coefficients derived from the dimensional analysis method and Buckingham π theorem are consistent with the similar criteria derived from the fluid–structure coupling model with uniform continuous media.

Table 1. Key physical dimensions and scaling relation.

Physical Parameter	Dimension	Similarity Relation
Density ρ	ML^{-3}	Basic control variable, $C_\rho = 1$
Geometric dimension L	L	Basic control variable, C_L
Acceleration a	LT^{-2}	Basic control variable, C_a
Elastic modulus E	$ML^{-1}T^{-2}$	$C_E = C_\rho C_L C_a$
Poisson's ratio μ	/	1
Cohesion c	$ML^{-1}T^{-2}$	$C_c = C_\rho C_L C_a$
Internal friction Angle φ	/	1
Stress σ	$ML^{-1}T^{-2}$	$C_\sigma = C_\rho C_L C_a$
Strain ε	/	1
Time t	T	$C_t = C_L^{0.5} C_a^{-0.5}$
Frequency ω	T^{-1}	$C_\omega = C_L^{-0.5} C_a^{0.5}$
Displacement x	L	$C_x = C_L$
Velocity v	LT^{-1}	$C_v = C_L^{0.5} C_a^{0.5}$
Gravitational acceleration g	LT^{-2}	$C_g = C_a$
Damping ratio λ	/	1
Dynamic elastic modulus Ed	$ML^{-1}T^{-2}$	$C_{E_d} = C_\rho C_L C_a$
Dynamic Poisson's ratio μd	/	1
External force F	MLT^{-2}	$C_E = C_\rho C_L^3 C_a$
Permeability coefficient k	LT^{-1}	$C_k = C_L^{0.5} C_a^{0.5}$
Softening coefficient η	/	1

3. Similar Material Ratio and Test Method

3.1. Selection of Similar Materials

According to the selection and matching principles of similar materials proposed by the relevant literature [24,34], (1) similar materials are mainly composed of granular materials and the molded samples are not easily affected by the external environment; (2) by changing the mix ratio of materials, the physical and mechanical properties of similar materials can be greatly changed to meet the needs of different similar conditions; and (3) the source of materials is wide, affordable, easy to form, nontoxic, and harmless. Therefore, 0.3–0.5 mm and 1.0–2.0 mm quartz sand and barite powder were selected as aggregates in this test. P.O. 42.5 cement and sodium silicate as cementing agents can widely adjust the hydraulic properties and strength of similar materials to ensure that the material does not disintegrate in contact with water. With rosin powder and glycerin as modulators, rosin is not soluble in water and has a certain bonding effect; glycerin has the role of moisturizing and reducing dry cracking. The basic components of similar materials selected in the test are shown in Figure 2.

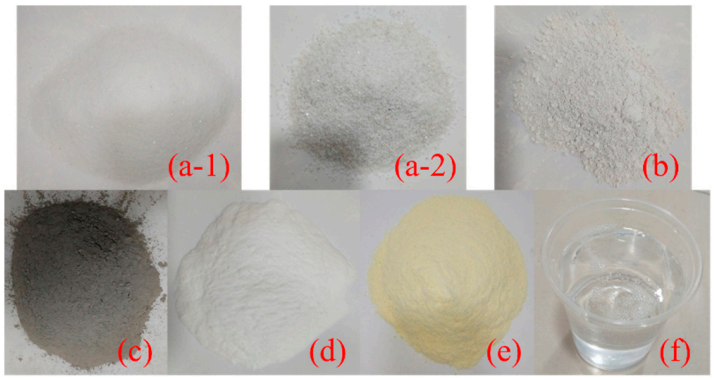

Figure 2. Similar material basic components of rock mass under seepage and dynamic coupling: (**a-1**) 0.3–0.5 mm quartz sand; (**a-2**) 1.0–2.0 mm quartz sand; (**b**) barite powder; (**c**) cement; (**d**) sodium silicate; (**e**) rosin; and (**f**) glycerinum.

3.2. The Ratio of Similar Materials

Orthogonal experimental design is a statistical method that selects the optimal test scheme according to certain rules under multifactor and multilevel conditions. It can efficiently find the law of the influence of various factors on the test results [35]. It has been widely used in the research of similar material ratio tests and many research results have been achieved [6,24,25].

Due to the large composition of materials in this test, to develop similar materials with a wider range of regulation, 6 factors were set in the experiment. Among them are the content of quartz sand of different particle sizes (factor A), the mass ratio of barite powder to quartz sand (factor B), the mass ratio of cement to quartz sand (factor C), the mass ratio of rosin to quartz sand (factor D), the mass ratio of sodium silicate to quartz sand (factor E), and the mass ratio of glycerin to quartz sand (factor F). Five levels were set for each factor. Factor A set the mass ratio of 0.3–0.5 mm and 1.0–2.0 mm quartz sand as 1:0, 3:1, 1:1, 1:3, and 0:1. Factor B was set to 25%, 20%, 75%, 1, and 2; Factor C was set to 10, 20, 30, 40, and 50%; Factor D was set to 0, 5, 10, 15, and 20%; Factor E was set to 0, 5, 15, 25, and 50%; and Factor F was set to 2, 4, 6, 8, and 10%. Based on the above factors and levels, to better carry out the proportioning test, a uniform orthogonal test table L25(5^6) [35] was used in the design, as shown in Table 2.

Table 2. Homogeneous orthogonal test table for similar materials $L_{25}(5^6)$.

Test Number	Factor						Test Scheme
	A	B	C	D	E	F	
1	1	1	5	3	4	2	$A_1B_1C_5D_3E_4F_2$
2	1	2	4	1	5	4	$A_1B_2C_4D_1E_5F_4$
3	1	3	2	5	1	3	$A_1B_3C_2D_5E_1F_3$
4	1	4	1	2	3	1	$A_1B_4C_1D_2E_3F_1$
5	1	5	3	4	2	5	$A_1B_5C_3D_4E_2F_5$
6	2	1	3	2	1	4	$A_2B_1C_3D_2E_1F_4$
7	2	2	5	5	2	1	$A_2B_2C_5D_5E_2F_1$
8	2	3	1	3	5	5	$A_2B_3C_1D_3E_5F_5$
9	2	4	4	4	4	3	$A_2B_4C_4D_4E_4F_3$
10	2	5	2	1	3	2	$A_2B_5C_2D_1E_3F_2$
11	3	1	2	4	5	1	$A_3B_1C_2D_4E_5F_1$
12	3	2	3	3	3	3	$A_3B_2C_3D_3E_3F_3$
13	3	3	4	2	2	2	$A_3B_3C_4D_2E_2F_2$
14	3	4	5	1	1	5	$A_3B_4C_5D_1E_1F_5$
15	3	5	1	5	4	4	$A_3B_5C_1D_5E_4F_4$
16	4	1	1	1	2	3	$A_4B_1C_1D_1E_2F_3$
17	4	2	2	2	4	5	$A_4B_2C_2D_2E_4F_5$
18	4	3	5	4	3	4	$A_4B_3C_5D_4E_3F_4$
19	4	4	3	5	5	2	$A_4B_4C_3D_5E_5F_2$
20	4	5	4	3	1	1	$A_4B_5C_4D_3E_1F_1$
21	5	1	4	5	3	5	$A_5B_1C_4D_5E_3F_5$
22	5	2	1	4	1	2	$A_5B_2C_1D_4E_1F_2$
23	5	3	3	1	4	1	$A_5B_3C_3D_1E_4F_1$
24	5	4	2	3	2	4	$A_5B_4C_2D_3E_2F_4$
25	5	5	5	2	5	3	$A_5B_5C_5D_2E_5F_3$

3.3. Preparation of Similar Materials and Testing of Physical and Mechanical Parameters

3.3.1. Preparation of Similar Materials

Similar material specimens were prepared according to the amount of quartz sand, barite powder, cement, and other materials in Table 2. To ensure the uniformity of the material after mixing, firstly, solid raw materials such as quartz sand and barite powder were mixed evenly. Then, the water was mixed evenly with glycerin and added to the solid raw material to stir fully (the water content was 12% of the mass of the specimen).

The similar material was poured into the mold in 3 layers and they were tamped. After tamping, the mixture was allowed to stand at room temperature for 24 h and the mold was then removed. The dismantled specimens were numbered and maintained at room temperature and natural drying for 7 days. Figure 3 shows 25 groups of test specimens with different proportions and 12 specimens in each group, totaling 300 specimens.

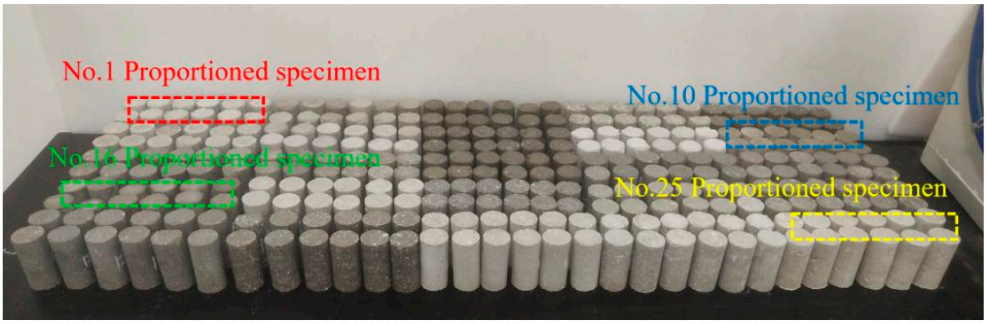

Figure 3. Partially specimen based on similar material.

3.3.2. Physical and Mechanical Parameter Testing of Similar Materials

The test was carried out in strict accordance with the uniform orthogonal test design scheme and relevant test procedure [36,37]. These 25 groups of samples based on the orthogonal test design were used to carry out weight measurements, uniaxial compression tests, triaxial tests, penetration tests, wave velocity tests, and softening coefficient tests. In the course of the test, a TSZ-10 triaxial instrument was used for uniaxial and triaxial tests, a falling head permeameter was used for the penetration test, and a CTS-25 ultrasonic detector was used for the wave velocity test. The test process and instruments are shown in Figure 4.

Figure 4. Testing process of experiments: (**a**) uniaxial and triaxial test instruments; (**b**) falling head permeability test; (**c**) longitudinal and shear wave monitoring; and (**d**) softening coefficient measurement.

The specific test process is as follows:

(1) Density measurement. Vernier calipers were used to measure the diameter of the specimen at the top, bottom ends, and middle 3 positions and the average value was taken. This value is the cross-sectional area of the specimen. The height of the specimen was measured and averaged. The specimen was weighed and measured and the mass was recorded. The corresponding result is obtained according to the density calculation formula. Each group of 12 samples was measured, the density was calculated, and finally, the average value was obtained;

(2) Uniaxial compressive strength measurement. The test specimen was placed on the TSZ triaxial apparatus and the position of the test piece was adjusted so that it was in the center of the base. Start the bearing table so that the specimen and the pressure sensor on the top of the triaxial meter are in contact with each other. The loading rate was controlled at 0.01 mm/s and the load was applied until the specimen was damaged. The relevant stress and strain data were recorded during the test (Figure 4a);

(3) Triaxial test. The equipment used in the test is still a TSZ triaxial instrument. The preset confining pressures are 100, 200, and 300 kPa, respectively. After the specimen is installed, the cap is raised to make contact with the top sensor. The triaxial test controlled the loading rate of 0.002 mm/s. After the specimen was damaged, the test was stopped and the relevant stress–strain data were analyzed. The cohesion and internal friction angles in Table 3 were calculated according to the envelope of the triaxial test (Figure 4a);

(4) Falling head permeameter. Considering that the permeability coefficient of different samples may be very different, a falling head permeameter was used to test and measure the permeability. The specimen was placed inside the sleeve. The valve of the water supply pipe was opened and recorded the head height at this time. When the water level of the water supply pipe dropped by more than 20 mm, the valve was closed and the height and corresponding time of the water head at this time were record. The permeability coefficient of the corresponding sample is calculated according to Darcy's law (Figure 4b);

(5) Softening coefficient test. The specimen was placed into the sink and water was added to the 1/2 height of the specimen. After 24 h, water continued to be added until the specimen was soaked in water and then it was soaked again for 24 h. The specimen was removed and the strength of the specimen was measured by the uniaxial test method. The ratio between the strength of the specimen after soaking and the strength in the natural state is the softening coefficient (Figure 4d). Physical and mechanical parameters such as the density compressive strength, elastic modulus, cohesion, internal friction angle, softening coefficient, and permeability coefficient of similar materials under multi-field coupling were obtained. The test results are shown in Table 3.

Table 3. Test results of similar materials.

Test Number	Density/ $g \cdot cm^{-3}$	Compressive Strength/ kPa	Elastic Modulus/ MPa	Cohesion/ kPa	Internal Friction Angle/°	Softening Coefficient/ %	Permeability Coefficient/ m/s	Dynamic Elastic Modulus/ GPa	Dynamic Poisson's Ratio
1	1.624	521.83	42.419	115.43	23.27	75.66	1.59×10^{-6}	7.18	0.215
2	1.597	656.77	24.734	214.12	21.57	92.62	1.95×10^{-7}	7.96	0.248
3	2.050	460.90	20.008	108.49	42.59	83.23	7.70×10^{-7}	7.49	0.241
4	2.149	951.10	55.044	213.05	39.62	97.86	1.20×10^{-6}	9.12	0.199
5	2.053	696.00	39.535	148.33	43.56	98.12	4.63×10^{-7}	4.24	0.203
6	1.948	202.33	9.360	40.26	38.51	67.12	2.37×10^{-6}	5.66	0.228
7	1.849	1007.15	52.875	148.52	49.55	82.44	2.77×10^{-6}	3.57	0.214
8	2.033	202.18	5.014	63.69	9.21	24.04	3.42×10^{-6}	3.40	0.259

Table 3. *Cont.*

Test Number	Density/ g·cm^{-3}	Compressive Strength/ kPa	Elastic Modulus/ MPa	Cohesion/ kPa	Internal Friction Angle/°	Softening Coefficient/ %	Permeability Coefficient/ m/s	Dynamic Elastic Modulus/ GPa	Dynamic Poisson's Ratio
9	1.816	624.83	39.825	135.8	24.75	21.99	1.01×10^{-8}	8.20	0.202
10	2.087	1571.50	100.652	162.47	46.35	59.47	3.37×10^{-6}	5.73	0.201
11	1.720	213.10	4.630	55.84	20.86	22.55	1.07×10^{-9}	5.84	0.229
12	1.839	842.73	50.731	37.55	36.01	37.51	4.28×10^{-6}	7.19	0.263
13	2.123	804.00	57.626	121.17	48.53	71.67	8.34×10^{-9}	5.84	0.211
14	2.261	980.13	54.597	284.01	36.77	90.94	1.26×10^{-6}	7.85	0.205
15	2.245	602.20	23.910	251.46	15.26	59.02	2.12×10^{-6}	6.42	0.242
16	2.158	121.80	7.063	113.33	35.98	89.75	7.19×10^{-7}	2.56	0.230
17	2.150	650.30	25.676	199.83	29.62	96.04	4.03×10^{-7}	7.75	0.242
18	1.883	1771.50	73.260	201.89	47.84	93.71	3.62×10^{-7}	5.86	0.271
19	1.844	528.33	19.768	162.85	21.16	38.01	2.18×10^{-6}	7.56	0261
20	2.195	731.83	48.912	99.57	46.59	94.58	1.77×10^{-6}	5.79	0.195
21	1.794	316.60	13.138	20.95	34.73	83.67	3.01×10^{-8}	5.58	0.247
22	2.064	182.04	10.631	93.89	33.88	98.75	3.86×10^{-7}	4.75	0.238
23	1.931	1244.40	66.527	358.85	37.71	82.72	2.60×10^{-6}	9.36	0.263
24	1.987	793.33	40.592	288.07	29.51	86.44	4.97×10^{-9}	3.84	0.214
25	1.904	922.84	60.660	346.83	23.75	61.56	1.77×10^{-6}	8.97	0.229

4. Sensitivity Analysis of Physical and Mechanical Parameters of Similar Materials

The range analysis method is often used in orthogonal tests. It has the characteristics of simple calculation and ease of understanding. The range analysis reflects the influence of a certain factor on the properties of materials. The range size reflects the influence of a certain factor on the properties of the material. Therefore, the influence degree of different factors on the test index can be intuitively judged through range analysis. In general, the greater the range is, the greater the influence of the factor on the physical properties of the material [35]. The following analysis uses range analysis to discuss the law of influence factors on the hydraulic and dynamic characteristics of the developed similar materials.

4.1. Sensitivity Analysis of Density-Influencing Factors

The mean value and range of factors at different levels in the uniform orthogonal test results are shown in Table 4. It can be seen from Table 4 that the range size is the factor C, E, B, A, D, and F in turn. This indicates that the content of Portland cement and sodium silicate plays a dominant role in the density of the specimen, followed by the content of barite powder, while the particle size, rosin, and glycerin content have little influence on the density.

Table 4. Analysis table of the density sensitivity factor.

Horizontal Groups	Density Test Result/g·cm^{-3}					
	A	B	C	D	E	F
1	1.895	1.849	2.130	2.007	2.104	1.969
2	1.947	1.900	1.999	2.055	2.034	1.948
3	2.038	2.004	1.923	1.936	1.951	1.953
4	2.046	2.011	1.546	1.907	1.953	1.932
5	1.936	2.097	1.904	1.956	1.783	2.058
Range/R	0.151	0.248	0.584	0.148	0.321	0.126

Additionally, the influence of various factors on the density of specimens is shown in Figure 5. Figure 5 shows that the specimen density increases with the increasing barite powder content, while the density decreases with increasing cement, sodium silicate, and other cementing agent content; the minimum value is obtained at a water–sand ratio of 40%. The other factors have little fluctuation and have little influence on the density of similar materials.

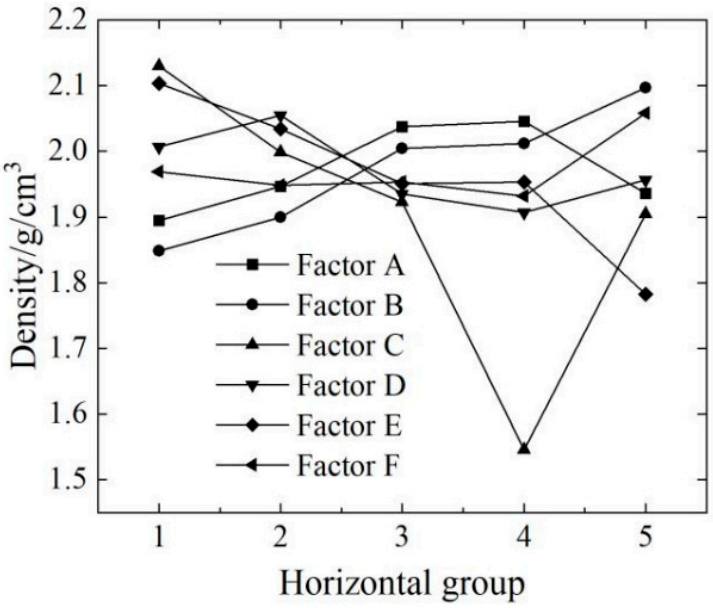

Figure 5. Sensitivity analysis of density.

4.2. Sensitivity Analysis of Influencing Factors of Compressive Strength

See Table 5 for the range of compressive strengths of similar materials calculated by various factors. The stress–strain curves of some specimens are shown in Figure 6. The calculation results in Table 5 show that the sensitivity of the influence of each factor on compressive strength from large to small is factor B > C > E > D > F > A, indicating that the mass ratio of barite powder to quartz sand will affect the internal structure of the specimen and greatly affect the compressive strength of the specimen. The quartz sand and barite powder are aggregate components and their particle size compositions are different. Therefore, the porosity of quartz sand and barite powder with different proportions is different, which affects the strength of the specimen [38].

Table 5. Analysis table of physical parameter sensitivity factors.

Range in Physical Parameters/R	Factor					
	A	B	C	D	E	F
Compressive strength/kPa	103.4	629.7	628.8	331.9	579.2	260.5
Elastic modulus/MPa	6.61	69.41	36.43	24.77	29.86	18.63
Cohesion/kPa	111.6	147.6	105.2	105.7	87.03	68.0
Internal friction angle/°	4.752	6.814	9.446	7.088	15.3	8.328
Softening coefficient	0.385	0.144	0.247	0.195	0.275	0.21
Permeability elastic modulus/10^{-6} m/s	1.54	0.97	1.98	1.97	1.06	0.66
Dynamic elastic modulus/GPa	1.885	1.949	1.552	1.989	3.773	1.119
Dynamic Poisson's ratio	0.019	0.035	0.072	0.019	0.022	0.020

Furthermore, Figure 7 shows the variation trend of the compressive strength of similar materials under the influence of various factors. The compressive strength increases gradually with increasing barite powder and cement content, as shown in Figure 7. With increasing sodium silicate content, the compressive strength first increases and then decreases and an inflection point occurs when the mass ratio is 15%. The compressive strength decreases with increasing glycerol and rosin content.

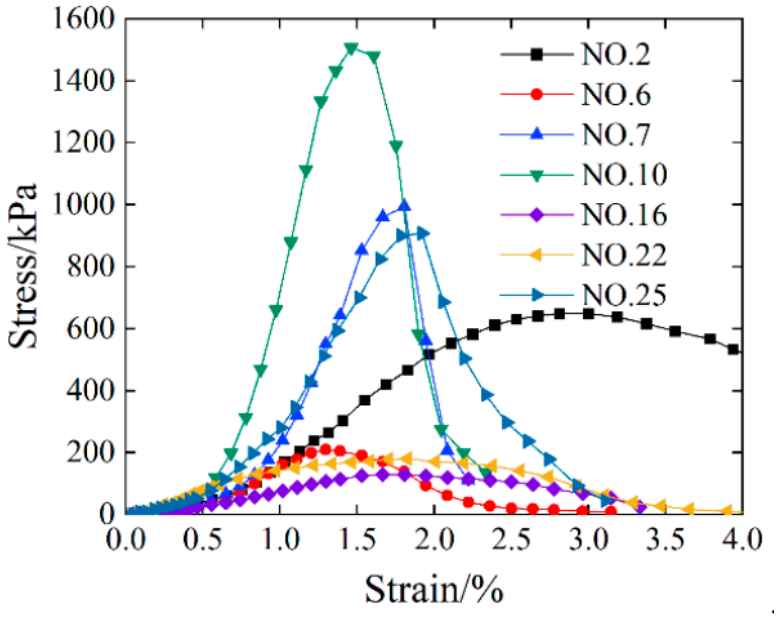

Figure 6. Stress–strain curves of specimens.

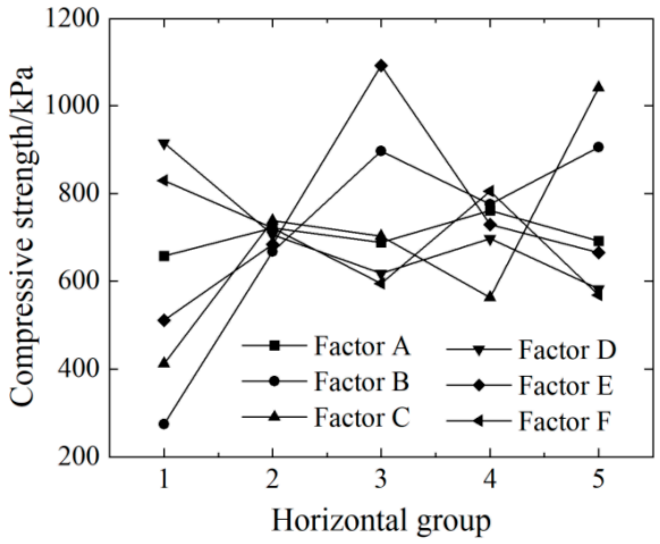

Figure 7. Sensitivity analysis of compressive strength.

4.3. Sensitivity Analysis of Influencing Factors of the Elastic Modulus

The elastic modulus is calculated according to the stress–strain curve obtained by the uniaxial test in this work. The range of factors affecting the test results of the elastic modulus is shown in Table 5. Table 5 shows that the range of factors B and C is significantly greater than other factors, indicating that the content of barite powder is the main control factor of the elastic modulus of similar materials.

The variation law of the elastic modulus with various factors is shown in Figure 8. Figure 8 shows that the variation trend of the elastic modulus with various factors is similar to that of compressive strength. It increases with increasing barite powder and cement contents and decreases with increasing rosin and glycerin contents. However, with increasing water glass content, its content first increases and then decreases and there is an inflection point when the mass ratio is 15%.

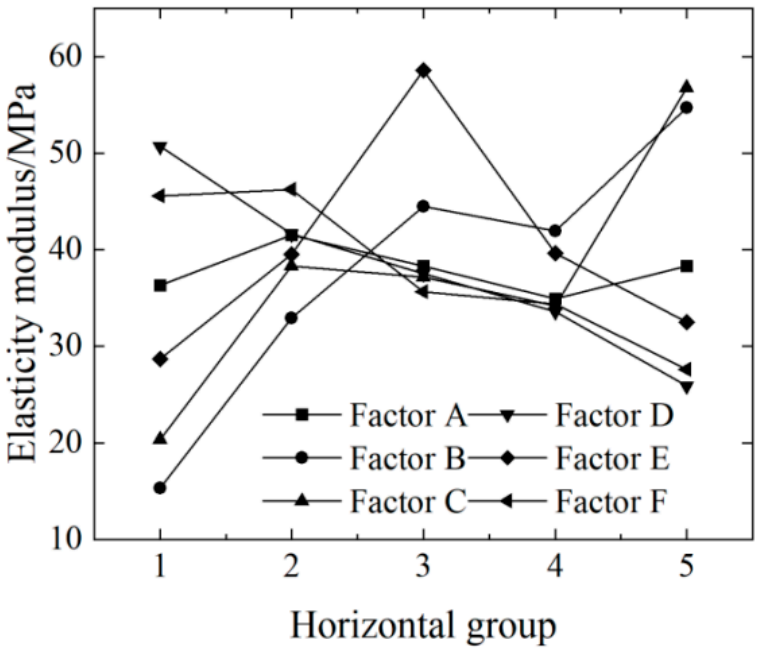

Figure 8. Sensitivity analysis of the elasticity modulus.

4.4. Sensitivity Analysis of Influencing Factors of Cohesion

Cohesion is obtained according to the stress circle drawn by the triaxial test in this work. The stress–strain curves and stress circles of some specimens are shown in Figure 9. The range difference in cohesion of similar materials under different factors was calculated and the results are shown in Table 5. Table 5 shows that factor B (content of barite powder) has the largest range, followed by factors D, C, A, E, and F.

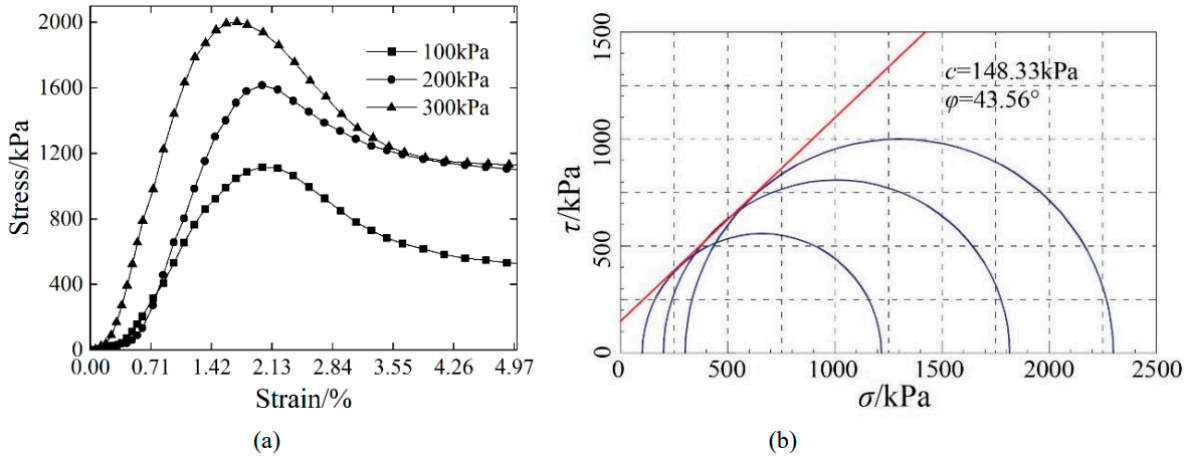

Figure 9. Triaxial curve and Mohr circle of the No.5 specimen. (**a**) Strain-stress curves; (**b**) stress circle.

Based on the calculation results of cohesion, the influence rules of various factors on the cohesion of specimens were obtained, as shown in Figure 10. In Figure 10, the barite powder content has a significant impact on cohesion. With the increase in binder content (Factors C and E), the cohesion fluctuates slowly at first and reaches an extreme value, indicating that binder content is helpful to improve the cementing property of materials. But with increasing rosin content, the cohesion of the specimens gradually decreases, which plays a weakening role in the change in cohesion.

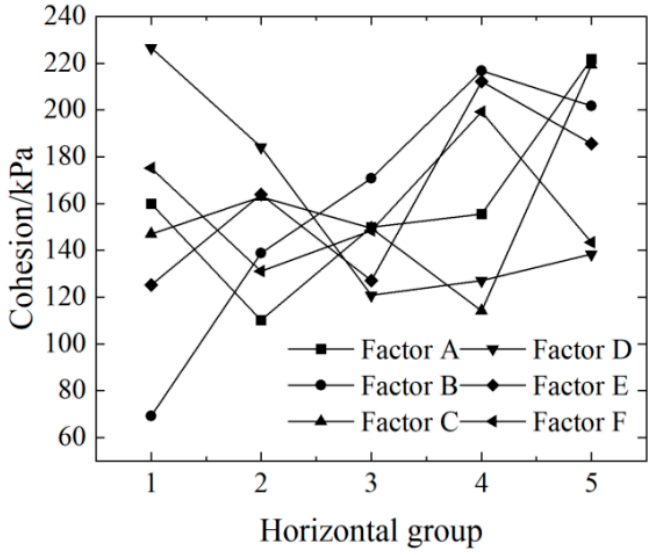

Figure 10. Sensitivity analysis of cohesion.

4.5. Sensitivity Analysis of Influencing Factors of the Internal Friction Angle

The internal friction angle is also calculated according to stress circles. The triaxial curve and stress circle of some specimens are also shown in Figure 9. Thus, the range of each factor affecting the test results of the internal friction angle is obtained. The results of factors A-F are shown in Table 5. The range of the internal friction angle from large to small is factors E, C, F, D, B, and A, among which the range of factor E is larger than that of the other factors and plays a major regulating role.

The changing trend of the internal friction angle of similar materials is shown in Figure 11. Figure 11 points out that the internal friction angle φ fluctuates slowly with increasing mass fraction of sodium silicate at first and then shows a sudden decreasing trend when the mass ratio is 25%. Additionally, because glycerin has lubricity, the cementation effect of materials will be weakened, so φ gradually decreases with increasing glycerin content. When the content of sodium silicate and glycerin (factors E and F) is high during the preparation of the specimen, the specimen is not easy to form and has a lower internal friction angle (for example, Group 8, etc.).

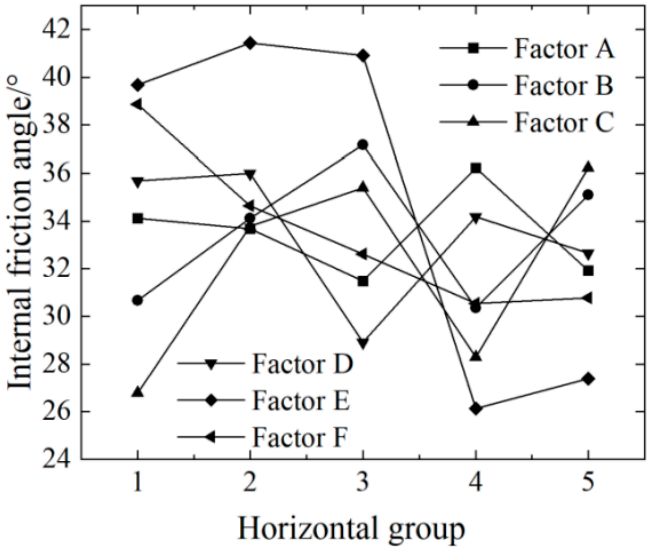

Figure 11. Sensitivity analysis of the friction angle.

4.6. Sensitivity Analysis of Influencing Factors of the Softening Coefficient

Similar materials will be soaked in water during the hydro-dynamic characteristic test and the material will inevitably deteriorate under the action of water. The softening coefficient η is one of the indicators to characterize the softening effect of rock, which refers to the ratio of uniaxial compressive strength in the saturated state to uniaxial compressive strength in the dry state. The smaller the softening coefficient, the stronger the softening effect of rock. The range of factors affecting the test results of the softening coefficient was obtained based on Table 3 and the range results of factors A–F are shown in Table 5. Table 5 shows that the range of particle size gradation (factor A) of quartz sand is larger than the content of binder, modifier, and quartz sand. This shows that the softening coefficient of the material is mainly regulated by the particle size of the quartz sand followed by the binder content and that the other factors have little fluctuation. Meanwhile, the variation trend of the softening coefficient of similar materials with various factors was plotted (Figure 12). When the particle size grading of quartz sand (factor A) is more uniform, there are fewer hydrophobic channels inside the specimen and the softening coefficient is smaller. However, when the grading is poor, there are more channels inside the specimen and the water will accelerate the softening of the specimen. The soft coefficient decreases with increasing sodium silicate content, which indicates that sodium silicate has good water resistance. However, the soft coefficient decreases first and then increases with increasing cement content and there is a turning point when the cement mass ratio is 30%. The softening coefficient of the material is also regulated by other rosin modulators.

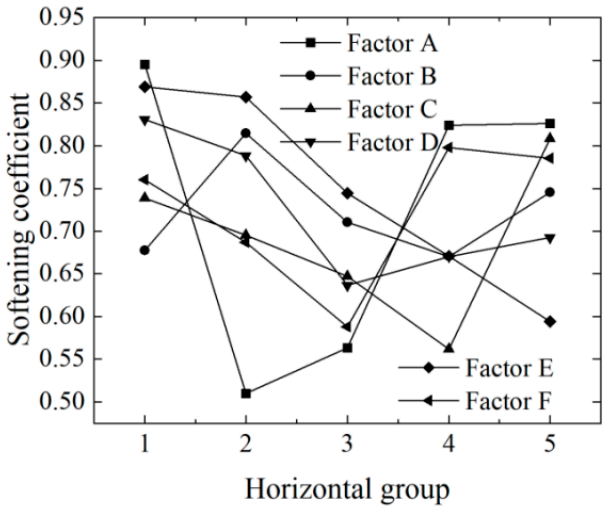

Figure 12. Sensitivity analysis of the softening coefficient.

4.7. Sensitivity Analysis of Influencing Factors of the Permeability Coefficient

The calculated range result of similar material permeability coefficients under various factors is shown in Table 5. The ranges of factors A-F are 1.54, 0.97, 1.98, 1.97, 1.06, and 0.66×10^{-6} m/s, respectively. Table 5 shows that cementing agents such as cement (factor C) play a main role in the permeability coefficient of similar materials. The particle size of quartz sand also plays a certain role in water infiltration, which is consistent with the sensitivity analysis of the softening coefficient [26]. Furthermore, the content of barite powder and glycerin does not play a significant role in regulating the permeability coefficient.

The variation trend of the permeability coefficient of similar materials with various factors is drawn, as shown in Figure 13. It can be seen from Figure 13 that cement, sodium silicate, and other cementing materials have the same change trend and their permeability coefficients reach the extreme value when the content is 40% and 5%. respectively. The influence of the particle size of quartz sand on the permeability coefficient is similar to that of the softening coefficient. When the gradation is poor, the internal pores of sim-

ilar materials will play a role in promoting water penetration. When the mass ratio of 0.3–0.5 mm to 1–2 mm quartz sand is 3:1, the permeability coefficient of similar materials has the maximum value. However, raw materials such as barite powder and glycerin have little fluctuation in the figure and have no obvious control effect on the permeability coefficient.

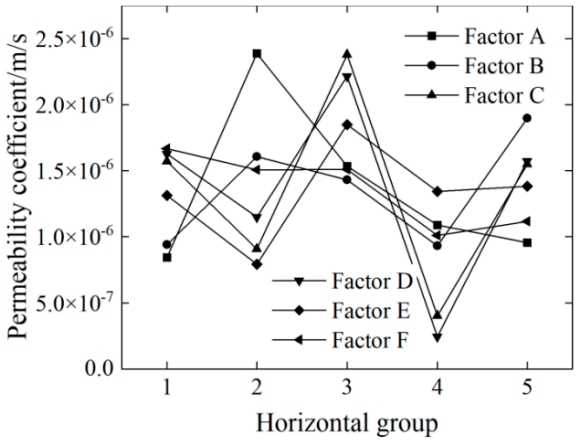

Figure 13. Sensitivity analysis of the permeability coefficient.

4.8. Sensitivity Analysis of Influencing Factors of Dynamic Elastic Modulus

In this work, the dynamic elastic modulus and dynamic Poisson ratio of similar materials are calculated by using the measured P-wave velocity and S-wave velocity and are derived by Equation (5):

$$\left.\begin{aligned} E_d &= \rho v_s^2 \frac{\left(3v_p^2 - 4v_s^2\right)}{\left(v_p^2 - v_s^2\right)} \\ \mu_d &= \frac{\left(v_p^2 - 2v_s^2\right)}{2\left(v_p^2 - v_s^2\right)} \end{aligned}\right\} \quad (5)$$

The range result of various factors affecting the dynamic elastic modulus is obtained, as shown in Table 5. The range is E, D, B, A, C, and F from largest to smallest, in which factor E (sodium silicate) has the maximum value. Table 5 indicates that factor E has a dominant role in the dynamic elastic modulus of similar materials. The changing trend of the dynamic elastic modulus of similar materials is shown in Figure 14. Figure 14 shows that the dynamic elastic modulus Ed first decreases and then increases with increasing sodium silicate content and the maximum value is obtained when the sodium silicate content is 25%. On the other hand, quartz sand and cement have little influence on the dynamic elastic modulus and the test results fluctuate in the range of 5–7 GPa.

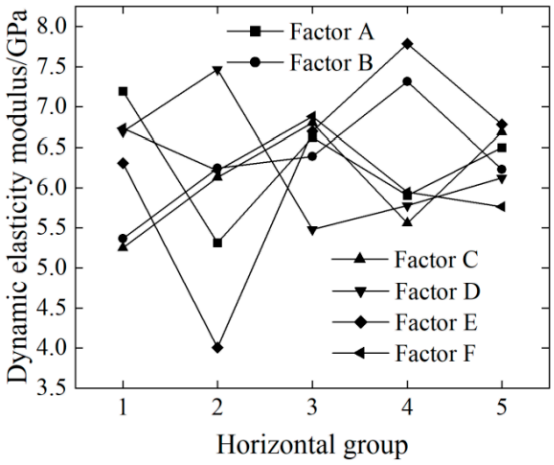

Figure 14. Sensitivity analysis of the dynamic elasticity modulus.

4.9. Sensitivity Analysis of Factors Influencing the Dynamic Poisson's Ratio

The range of factors influencing the results of the dynamic Poisson's ratio was obtained. In Table 5, the results of factors A-F were 0.01911, 0.03532, 0.07248, 0.01912, 0.02196, and 0.0202, respectively. Thus, the range of factor C (cement) was the largest, followed by factors B, E, F, D, and A. According to the calculation results of the dynamic Poisson's ratio μd, a line chart of the influence of various factors on the dynamic Poisson's ratio of the specimen was made, as shown in Figure 15.

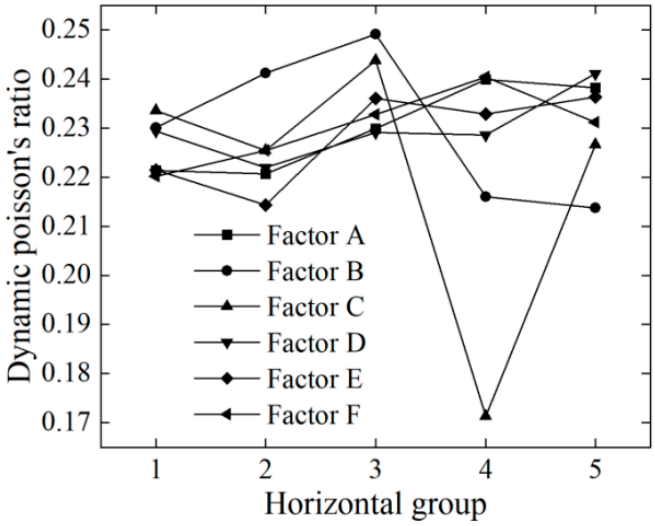

Figure 15. Sensitivity analysis of dynamic Poisson's ratio.

In Figure 15, the fluctuation of factor C is the most obvious; that is, the cement content has a great influence on the dynamic Poisson's ratio. With the increase in the cement-to-quartz sand mass ratio, dynamic Poisson's ratio curve presents a W-shaped change and reaches a minimum value at a mass ratio of 40%. Factor B (barite powder) also has a certain adjustment effect on the dynamic Poisson's ratio with the increase in the content of μd first increasing and then decreasing. The μd increased with increasing the other factors' content but the overall change was small.

4.10. Statistical Regression Analysis of Physical and Mechanical Parameters

Through the analysis of the test results, it can be found that the density, elastic modulus, and other physical parameters of similar materials can be changed over a large range. To facilitate the selection of the ratio of similar materials, multiple linear regression analysis is used to establish the relationship between physical parameters and the ratio of each component of similar materials. The following uses SPSS software (version 26.0) to conduct multiple linear regression analyses of the key physical parameters of the experiment. Among them, A, B, C, D, E, and F are the particle size mass ratios of 0.3–0.5 mm and 1–2 mm of quartz sand and the mass ratios of barite powder, cement, rosin, sodium silicate and glycerin to quartz sand, respectively. Through multiple linear regression analysis, we can obtain:

Formula (6) provides an empirical formula for obtaining the appropriate ratio of similar materials. On this basis, fine-tuning the ratio and comparing the actual measured physical parameters with the actual values can effectively reduce the time for obtaining the optimal proportion.

$$\begin{bmatrix} \rho \\ \sigma \\ E \\ c \\ \varphi \\ \eta \\ k \\ E_d \\ \mu_d \end{bmatrix} = \begin{bmatrix} -0.073 & 0.135 & -0.545 & -0.497 & -0.517 & 0.812 \\ -43.28 & 269.85 & 1146.63 & -1344.765 & -232.25 & -2186.32 \\ 1.074 & 18.959 & 71.394 & -115.294 & -24.415 & -239.295 \\ -67.606 & 64.378 & 94.886 & -466.564 & 84.048 & 21.95 \\ 0.739 & 1.362 & 20.34 & -15.728 & -47.258 & -101.38 \\ -0.071 & 0.008 & 0.173 & -0.79 & -0.806 & 0.806 \\ 4.3 \times 10^{-7} & 3.9 \times 10^{-7} & -5.4 \times 10^{-7} & -2.03 \times 10^{-7} & 7.37 \times 10^{-7} & -8.01 \times 10^{-7} \\ 0.32 & 0.351 & 3.426 & -5.639 & 3.385 & -11.066 \\ -0.021 & -0.015 & -0.019 & 0.06 & -0.054 & -0.185 \end{bmatrix} \cdot \begin{bmatrix} A \\ B \\ C \\ D \\ E \\ F \end{bmatrix} + \begin{bmatrix} 2.15 \\ 448.558 \\ 29.395 \\ 134.717 \\ 42.424 \\ 0.884 \\ 1.5 \times 10^{-6} \\ 5.389 \\ 0.232 \end{bmatrix} \quad (6)$$

5. Damage Pattern Analysis of Similar Materials

To ensure that specimens made of similar materials and natural rocks have similar failure characteristics under loading, the failure forms and characteristics of specimens with different proportions under uniaxial compression are statistically analyzed. The failure patterns of 25 groups of tests are shown in Figure 16. The statistics of the failure patterns of the samples in each group are shown in Table 6.

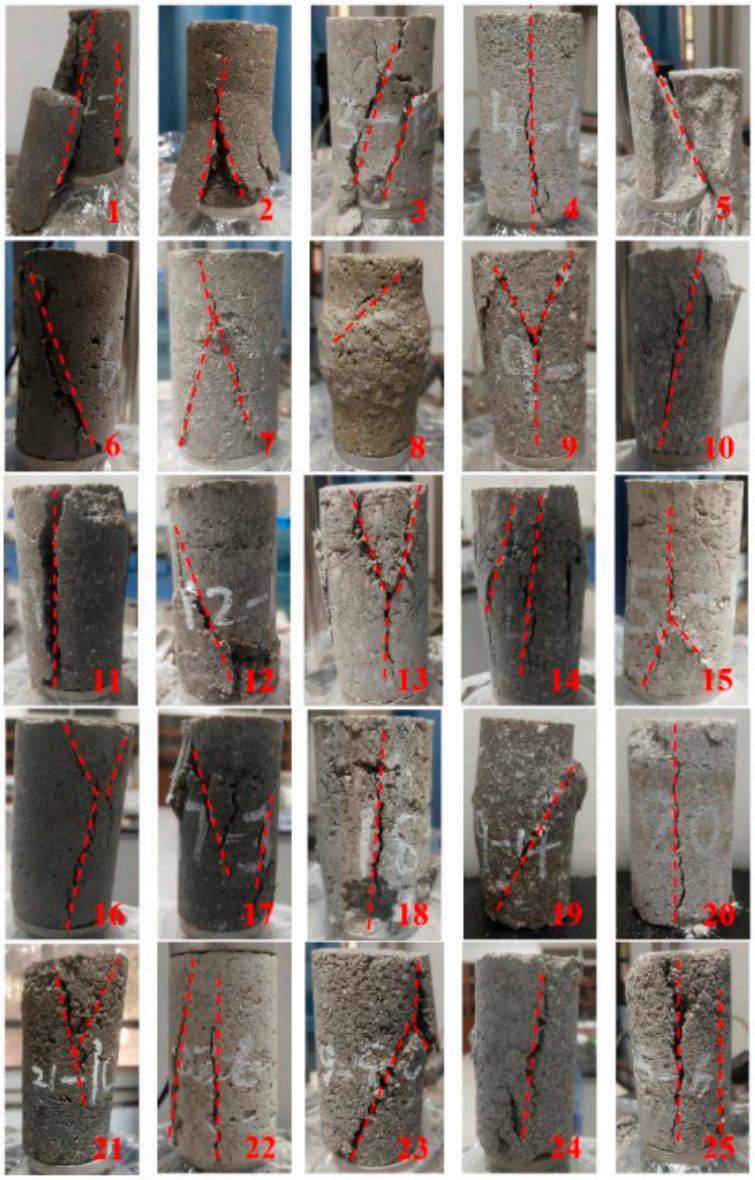

Figure 16. Specimen failure mode.

Table 6. Failure mode statistic of the specimen.

Failure Mode	The Number of the Orthogonal Test
Conical failure	2, 7, 9, 13, 15, 16, 21, 23
Tension splitting failure	1, 4, 10, 11, 14, 18, 20, 22, 24, 25
Oblique shear failure	3, 5, 6, 12, 19
Compound failure	8, 17

As shown in Figure 16 and Table 6, there are 10 groups of tensile and splitting failure, 8 groups of conical failure, 5 groups of oblique shear failure, and 2 groups of composite failure modes. These phenomena show that different material ratios can simulate different types of failure modes.

Meanwhile, the reasons for the above phenomena are as follows: under ideal conditions, the test specimen is in a one-dimensional compression state under vertical pressure, that is, under vertical pressure and transverse expansion. Since the tensile strength of the brittle material is far less than the compressive strength, the test specimen will undergo tensile splitting failure. In the actual test, the test specimen produces a conical fracture surface due to the friction between the end and the pressure plate and the fracture surface splits the remaining part under the action of pressure, that is, the test specimen has conical failure. Therefore, 18 specimens exhibit tensile splitting and conical failure, accounting for 72% of the 25 similar materials with different proportions. Furthermore, when the end of the test block has local tensile shear cracks and the cracks extend into the main shear fracture plane, the test block will experience inclined shear failure, which is relatively rare. In the course of the test, the compound failure form may be due to the existence of more sodium silicate or glycerin in the specimen itself, which makes it exhibit a certain dilatancy effect.

6. Discussions

Previous studies have generally focused on the impact of a single factor, such as dynamic (earthquake, blasting, etc.) or hydraulic (rainfall, groundwater level, etc.) factors, on engineering projects; the similar materials developed thus mainly consider the impact of a single factor. However, as more and more engineering construction projects begin to face the problem of multi-field coupling such as pertaining to hydraulic and dynamic parameters, it is urgent to develop new similar materials that consider hydraulic and dynamic properties. In view of this, this paper designed the relevant experiment. Compared with previous studies, this experiment not only considered the hydraulic characteristics of the material but also studied the multi-field physical and mechanical parameters of the material.

According to the similarity relation formula in Section 2, the similarity relation of major physical parameters of similar materials is derived based on the dimensionless criterion and the Buckingham π theorem (Table 1). The formula can provide a basis for the calculation of physical model materials under hydraulic–dynamic coupling. The formula is consistent with the permeability coefficient similarity relationship derived by Zhang et al. based on the fluid–structure coupling equation. Based on the orthogonal test, a test scheme of six factors and five levels was designed. A new type of similar material with quartz sand and barite powder as aggregates, cement and sodium silicate powder as cementing materials, and rosin and glycerin as modulating agents was developed. The hydrodynamic properties, dynamic properties, and basic physical parameters of the material were fully studied. The developed similar materials have a wide range of parameters, with densities ranging from 1.597 to 2.261 g/cm^3. The compressive strength is 121.8~1771.5 kPa; the elastic modulus 4.63~100.65 MPa; the cohesion is 20.95~358.85 kPa; the internal friction angle is 9.21~49.55°; the softening coefficient is 0.22~0.98; the permeability coefficient is 1.07×10^{-9}~4.28×10^{-6} m/s; the dynamic elastic modulus is 2.56~9.36 GPa; and the dynamic Poisson's ratio ranges from 0.195 to 0.271. The sensitivity of the physical parameters of similar materials was analyzed by range analysis. The results show that the main

parameters affecting the compressive strength, elastic modulus, and cohesion of similar materials are the content of barite powder. The main parameter affecting density and the dynamic Poisson ratio was the cement content. The rosin content has a certain influence on the internal friction angle and dynamic elastic modulus of similar materials. The particle size of quartz sand mainly affects the softening coefficient of similar materials. The change in the permeability coefficient is mainly controlled by cement and sodium silicate.

All these results show that the newly developed similar materials can satisfy the physical model tests under the action of hydrodynamic coupling. For example, the surrounding rock and lining structures can be constructed with similar materials of different proportions to study the dynamic response characteristics of the water-rich tunnel. Slope rock masses with cracks can be constructed by laying blocks with similar materials in advance and the infiltration characteristics of slopes under the action of rainfall can be studied. In the field of coal mining or backfill, the instability of underground reservoirs or the failure phenomenon under the coupling action of reservoir water and mine earthquakes can be simulated. In addition, although this study has conducted relevant research on the hydraulic and dynamic characteristics of new similar materials, there are still shortcomings in the coupling analysis of materials. In the later stage, the mechanical properties of similar materials under different water contents can be explored so as to obtain the physical and mechanical properties under different water contents, laying the foundation for the theoretical calculation of the later physical model.

7. Conclusions

In this work, the hydraulic and dynamic properties and failure modes of similar materials in physical rock mass models are studied.

(1) The similarity relationship of similar materials in a rock mass under seepage and dynamic coupling is derived based on the dimensionless criterion and Buckingham π theorem with density, geometry, and acceleration as control variables;
(2) A similar material ratio scheme with quartz sand and barite powder as aggregates, cement and water glass powder as cementing materials, and rosin and glycerin as modulators was established. It can satisfy both physical and mechanical properties as well as hydraulic properties and has a wide range of parameters, which can meet the ratio requirements of various geotechnical model tests;
(3) The sensitivity of the physical properties of similar materials to each parameter is analyzed. The empirical formula of the physical property parameters of similar materials is established based on multiple linear regression analysis.

Author Contributions: Validation, B.L.; Investigation, N.H.; Data curation, C.X.; Writing—original draft, W.S.; Writing—review & editing, J.Z.; Funding acquisition, D.S. All authors have read and agreed to the published version of the manuscript.

Funding: This study was funded by the National Natural Science Foundation of China (52109125), the China Postdoctoral Science Foundation (2020M680583), and the National Postdoctoral Program for Innovative Talent of China (BX20200191).

Institutional Review Board Statement: Not applicable.

Informed Consent Statement: Not applicable.

Data Availability Statement: All data used during the study are available from the corresponding author by request.

Acknowledgments: We would like to express our gratitude to the editors and reviewers for their constructive and helpful review comments.

Conflicts of Interest: The authors declare that they have no known competing financial interests or personal relationships that could have appeared to influence the work reported in this paper.

References

1. Li, S.-C.; Liu, H.-L.; Li, L.-P.; Zhang, Q.-Q.; Wang, K.; Wang, K. Large scale three-dimensional seepage analysis model test and numerical simulation research on undersea tunnel. *Appl. Ocean Res.* **2016**, *59*, 510–520. [CrossRef]
2. Zhang, D.; Sun, Z.; Fang, Q. Scientific problems and research proposals for Sichuan–Tibet railway tunnel construction. *Undergr. Space* **2021**, *7*, 419–439. [CrossRef]
3. Zhang, D.; Wang, J.; Qi, L.; Zhang, Y.; Ma, J.; Lu, G. Initiation and movement of a rock avalanche in the Tibetan Plateau, China: Insights from field observations and numerical simulations. *Landslides* **2022**, *19*, 2569–2591. [CrossRef]
4. Callisto, L.; Ricci, C. Interpretation and back-analysis of the damage observed in a deep tunnel after the 2016 Norcia earthquake in Italy. *Tunn. Undergr. Space Technol.* **2019**, *89*, 238–248. [CrossRef]
5. Häusler, M.; Gischig, V.; Thöny, R.; Glueer, F.; Donat, F. Monitoring the changing seismic site response of a fast-moving rockslide (Brienz/Brinzauls, Switzerland). *Geophys. J. Int.* **2022**, *229*, 299–310. [CrossRef]
6. Shen, X.; Yuan, D.; Cao, Y.; Gao, Z. Experiments on material proportions for simulating sandy layer in deep sea. *J. Southwest Jiaotong Univ.* **2020**, *55*, 628–634. [CrossRef]
7. Shan, Z.; Xie, Z.; Dong, R.; Jing, L. An analytical solution for the dynamic response of a seawater-sloping seabed-bedrock system under an oblique incident P wave. *Int. J. Numer. Anal. Methods Géoméch.* **2023**, *47*, 2136–2152. [CrossRef]
8. Li, Z.; Chen, T.; Liu, H.; Ji, C.; Zhu, C.; Hu, C.; Jia, Y. Earthquake response and post-earthquake stability assessment of submarine clay slopes. *Appl. Ocean Res.* **2022**, *127*, 18. [CrossRef]
9. Song, D.; Liu, X.; Li, B.; Zhang, J.; Bastos, J.J.V. Assessing the influence of a rapid water drawdown on the seismic response characteristics of a reservoir rock slope using time–frequency analysis. *Acta Geotech.* **2021**, *16*, 1281–1302. [CrossRef]
10. Menéndez, J.; Schmidt, F.; Konietzky, H.; Fernández-Oro, J.M.; Galdo, M.; Loredo, J.; Díaz-Aguado, M.B. Stability analysis of the underground infrastructure for pumped storage hydropower plants in closed coal mines. *Tunn. Undergr. Space Technol.* **2019**, *94*, 103117. [CrossRef]
11. Zhang, C.; Wang, F.; Bai, Q. Underground space utilization of coalmines in China: A review of underground water reservoir construction. *Tunn. Undergr. Space Technol.* **2020**, *107*, 103657. [CrossRef]
12. Abd, S.M.; Mhaimeed, I.S.; Tayeh, B.A.; Najm, H.M.; Qaidi, S. Investigation of the use of textile carbon yarns as sustainable shear reinforcement in concrete beams. *Case Stud. Constr. Mater.* **2023**, *18*, e01765. [CrossRef]
13. Tayeh, B.A.; Akeed, M.H.; Qaidi, S.; Abu Bakar, B. Ultra-high-performance concrete: Impacts of steel fibre shape and content on flowability, compressive strength and modulus of rupture. *Case Stud. Constr. Mater.* **2022**, *17*, e01615. [CrossRef]
14. Kongar-Syuryun, C.; Tyulyaeva, Y.; Khairutdinov, A.M.; Kowalik, T. Industrial waste in concrete mixtures for construction of un-derground structures and minerals extraction. In *IOP Conference Series: Materials Science and Engineering*; IOP Publishing: Bristol, UK, 2020; p. 032004.
15. Kongar-Syuryun, C.; Ubysz, A.; Faradzhov, V. Models and algorithms of choice of development technology of deposits when selecting the composition of the backfilling mixture. In *IOP Conference Series: Earth and Environmental Science*; IOP Publishing: Bristol, UK, 2021; p. 012008.
16. Kongar-Syuryun, C.; Faradzhov, V.; Tyulyaeva, Y.; Khayrutdinov, A. Effect of activating treatment of halite flotation waste in backfill mixture preparation. *Min. Inform. Anal. Bull.* **2021**, *1*, 43–57. [CrossRef]
17. Khayrutdinov, M.; Kongar-Syuryun, C.; Khayrutdinov, A.; Tyulyaeva, Y. Improving Safety when Extracting Water-soluble Ores by Optimizing the Parameters of the Backfill Mass. *Occup. Saf. Ind.* **2021**, *2021*, 53–59. [CrossRef]
18. Cao, L.; Zhang, J.; Wang, Z.; Liu, F.; Liu, Y.; Zhou, Y. Dynamic response and dynamic failure mode of the slope subjected to earthquake and rainfall. *Landslides* **2019**, *16*, 1467–1482. [CrossRef]
19. Zhang, Z.; Zhang, Q.; Xiang, W.; Yin, X.; Xue, T.; Lin, H.; Cheng, L.; Guo, X. Development and application of new-style hydro-mechanical coupling similar materials in complex environment. *J. Cent. South Univ. Sci. Technol.* **2021**, *52*, 4168–4180. [CrossRef]
20. Ads, A.; Iskander, M.; Bless, S.; Omidvar, M. Visualizing the effect of Fin length on torpedo anchor penetration and pullout using a transparent soil. *Ocean Eng.* **2020**, *216*, 108021. [CrossRef]
21. Tatone, B.S.; Abdelaziz, A.; Grasselli, G. Example framework for evaluation of synthetic rock-like materials as applied to a commercial gypsum cement. *Int. J. Rock Mech. Min. Sci.* **2023**, *169*, 105445. [CrossRef]
22. Li, S.C.; Feng, X.D.; Li, S.C.; Li, L.P.; Li, G.Y. Research and development of a new similar material for solid-fluid coupling and its application. *Chin. J. Rock Mech. Eng.* **2010**, *29*, 281–288.
23. Bai, J.; Wang, M.; Zhang, Q.S.; Zhu, Z.; Liu, R.; Li, W. Development and application of a new similar material for underground engineering fluid-solid coupling model test. *Chin. J. Rock Mech. Eng.* **2012**, *31*, 1128–1137.
24. Xu, Z.; Luo, Y.; Chen, J.; Su, Z.; Zhu, T.; Yuan, J. Mechanical properties and reasonable proportioning of similar materials in physical model test of tunnel lining cracking. *Constr. Build. Mater.* **2021**, *300*, 123960. [CrossRef]
25. Wang, H.; Zhao, M.; Zhong, Z.; Zhang, X.; Zhao, L.; Du, X. Similar materials for quasi-static scaled tests of fault-crossing tunnels. *Eng. Mech.* **2022**, *39*, 21–30. [CrossRef]
26. Shi, X.; Liu, B.; Qi, Y. Applicability of similar materials bonded by cement and plaster in solid-liquid coupling tests. *Rock Soil Mech.* **2015**, *36*, 2624–2630. [CrossRef]
27. Yang, X.; Su, D.; Zhou, B.; Zhen, L.; Zhou, C. Experiment study on similarity ratio of similar material for model test on red-bed soft rock. *Rock Soil Mech.* **2016**, *37*, 2231–2237. [CrossRef]

28. Tian, Q.; Zhang, J.; Zhang, Y. Similar simulation experiment of expressway tunnel in karst area. *Constr. Build. Mater.* **2018**, *176*, 1–13. [CrossRef]
29. Li, G.; Ma, F.S.; Guo, J.; Zhao, H.J. Experimental study on similar materials ratio used in large-scale engineering model test. *J. Northeast. Univ.* **2020**, *41*, 1653–1660. [CrossRef]
30. Tian, J.; Wang, L.; An, C.; Wu, Q.; Sun, Z.; Ke, R. Development of a Model Material for Dynamic Geotechnical Model Tests. *Appl. Sci.* **2022**, *12*, 5344. [CrossRef]
31. Yang, H.; Cui, S.; Pei, X.; Fan, X.; Lei, J. Multiple earthquake-induced progressive failure of bedding slopes with a saturated weak layer: Shaking table model tests. *Soil Dyn. Earthq. Eng.* **2023**, *170*, 107906. [CrossRef]
32. Fan, G.; Zhang, L.-M.; Zhang, J.-J.; Yang, C.-W. Time-frequency analysis of instantaneous seismic safety of bedding rock slopes. *Soil Dyn. Earthq. Eng.* **2017**, *94*, 92–101. [CrossRef]
33. Yue, Z.; Ye, Y.; Wang, Q.; Yao, N.; Shi, Y. A model for calculation of compressive strength of rock-like materials based on dimensional analysis. *Rock Soil Mech.* **2018**, *39*, 216–221. [CrossRef]
34. Zhou, Y.; Li, S.; Li, L.; Zhang, Q.; Shi, S.; Song, S.; Wang, K.; Chen, D.; Sun, S. New technology for fluid-solid coupling tests of underground engineering and its application in experimental simulation of water inrush in filled-type karst conduit. *Chin. J. Geotech. Eng.* **2015**, *37*, 1232–1240. [CrossRef]
35. Fang, K.; Ma, C. *Orthogonal and Uniform Experimental Design*; Science Press: Beijing, China, 2001; p. 248.
36. Standard for Test Methods of Engineering Rock Mass. *Ministry of Housing and Urban-Rural Development of the People's Republic of China*; General Administration of Quality Supervision, Inspection and Quarantine of the People's Republic of China: Beijing, China, 2013; p. 132.
37. Standard for Geotechnical Test Methods. *Ministry of Housing and Urban-Rural Development of the People's Republic of China*; State Administration for Market Regulation: Beijing, China, 2019; p. 717.
38. Shen, W.; Liu, S.; Xu, W.; Shao, J. An elastoplastic damage constitutive model for rock-like materials with a fractional plastic flow rule. *Int. J. Rock Mech. Min. Sci.* **2022**, *156*, 105140. [CrossRef]